Core/Shell Structured Hollow Mesoporous Nanocapsules: A Potential Platform for Simultaneous Cell Imaging and Anticancer Drug Delivery

Yu Chen,[†] Hangrong Chen,[†,*] Deping Zeng,[‡] Yunbo Tian,[‡] Feng Chen,[†] Jingwei Feng,[†] and Jianlin Shi*

[†]State Laboratory of High Performance Ceramic and Superfine Microstructure, Shanghai Institute of Ceramics, Chinese Academy of Sciences, Shanghai 200050, China, and [‡]Department of Biomedical Engineering, Chongqing Medical University, Chongqing 400016, China

ABSTRACT A potential platform for simultaneous anticancer drug delivery and MRI cell imaging has been demonstrated by uniform hollow inorganic core/shell structured multifunctional mesoporous nanocapsules, which are composed of functional inorganic (Fe_3O_4, Au, *etc.*) nanocrystals as cores, a thin mesoporous silica shell, and a huge cavity in between. The synthetic strategy for the creation of huge cavities between functional core and mesoporous silica shell is based on a structural difference based selective etching method, by which solid silica middle layer of Fe_2O_3@SiO_2@$mSiO_2$ (or Au@SiO_2@$mSiO_2$) composite nanostructures was selectively etched away while the mesoporous silica shell could be kept relatively intact. The excellent biocompatibility of obtained multifunctional nanocapsules (Fe_3O_4@$mSiO_2$) was demonstrated by very low cytotoxicity against various cell lines, low hemolyticity against human blood red cells and no significant coagulation effect against blood plasma. The cancer cell uptake and intracellular location of the nanocapsules were observed by confocal laser scanning microscopy and bio-TEM. Importantly, the prepared multifunctional inorganic mesoporous nanocapsules show both high loading capacity (20%) and efficiency (up to 100%) for doxorubicin simultaneously because of the formation of the cavity, enhanced surface area/pore volume and the electrostatic interaction between DOX molecules and mesoporous silica surface. Besides, the capability of Fe_3O_4@$mSiO_2$ nanocapsules as contrast agents of MRI was demonstrated both *in vitro* and *in vivo*, indicating the simultaneous imaging and therapeutic multifunctionalities of the composite nanocapsules. Moreover, the concept of multifunctional inorganic nanocapsules was extended to design and prepare Gd—Si—DTPA grafted Au@$mSiO_2$ nanocapsules for nanomedical applications, further demonstrating the generality of this strategy for the preparation of various multifunctional mesoporous nanocapsules.

KEYWORDS: mesoporous silica · nanocapsules · drug delivery · MRI · Fe_3O_4 · Au

Capsules, a common morphology with ultrathin shells and ultralarge cavities, have been commercially used as effective carriers for drug delivery, especially for oral drug administration. However, the extremely large particulate sizes (in milli- or centimeters) of commercial capsules severely limited their manipulation for intravenous drug administration, which has been generally considered as the most effective chemotherapeutic mode for serious diseases. The key that has fascinated biomedical researchers is how to design and control the sizes of capsules into the micro- and nanoscale, which might be solved by seeking help from chemistry. The emergence and development of nanotechnology have created a chance for reducing the sizes of the capsules into the micro/nano- scale range, making the intravenous drug administration of capsules possible. A large number of micro/nano- capsules, including organic,[1−3] inorganic,[4,5] and inorganic/organic hybrid ones,[6,7] have been developed as drug delivery systems (DDSs) for transporting therapeutic agents to lesion sites in the past decade. The biocompatible and biodegradable nature of polymer based capsules, generally fabricated by the layer-by-layer self-assembly technique,[7−12] showed great potential application in chemotherapy of serious diseases such as cancer and HIV.[13−17] The intrinsic instable nature of organic systems, unfortunately, still cast a shadow on their further clinical use. Alternatively, inorganic capsules with biocompatible and biodegradable features, especially porous ones, such as mesoporous silica,[4] mesoporous carbon,[18] carbon nanotube,[19] Fe_3O_4 aggregates[20,21] and $CaCO_3$,[22] exhibited various advantages compared to organic ones in their high chemical/thermal stability, high drug loading capability, sustained drug release from the supports and rich surface chemical functionalities for possible molecular recognition and targeted delivery, *etc.*

On the other hand, the multifunctionalization of capsules may enable the development of multifunctional nanomedical platforms for simultaneous imaging diagnosis and therapy.[23,24] The general methodology to achieve multifunctionalities on capsules

*Address correspondence to jlshi@sunm.shcnc.ac.cn, hrchen@mail.sic.ac.cn.

Received for review July 4, 2010 and accepted August 31, 2010.

Published online September 3, 2010. 10.1021/nn1015117

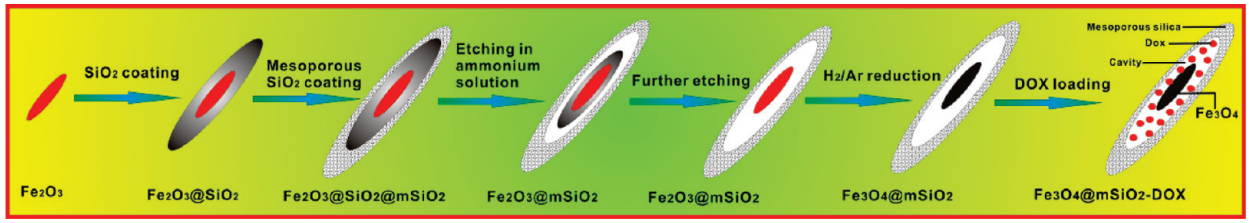

Scheme 1. Schematic Representation for the Preparation of Hollow Core/Shell Structured Mesoporous Nanocapsules with Magnetic Fe_3O_4 as the Core and Thin Mesoporous Silica Layer As the Shell[a] [a]Ellipsoidal Fe_2O_3 nanocrystals were coated by solid and mesoporous silica layer by traditional sol-gel process. Then, the fabricated composite nanoellipsoidals were etched in ammonium solution to partially or entirely remove the middle solid silica layer to prepare rattle-type (or yolk-shell type) nanocapsules using the structural difference between solid silica layer and mesoporous silica layer. After H_2/Ar reduction, the Fe_2O_3 core could be converted into magnetic Fe_3O_4. DOX molecules could be encapsulated into mesopores and cavities in the prepared magnetic nanocapsules.

is to add diverse functional inorganic nanocrystals into the cavity part of the capsules or to chemically graft functional groups onto the shells based on the rational/elaborate design in nanoscale. These inorganic nanocrystals can be Au,[25−32] Ag,[33] quantum dots (QDs),[34,35] Fe_3O_4 magnetic nanoparticles,[36−38] and the functional groups can be fluorescent molecules[39] or targeting molecules such as folic acid, *etc.*, endowing capsules with unique optical, acoustic and magnetic properties for clinical multi-imaging purposes (CT, MRI, US, PET, *etc.*) or targeting features for drug delivery. So far, however, the combined functionalities between physical imaging, such as MRI for cancer diagnosis, and an enhanced anticancer drug delivery property (e.g., high drug loading amount and efficiency) have been rarely reported.[23,36,37] Such a combination, as we believe, is greatly important because it allows simultaneous imaging diagnosis and drug delivery in one.

Herein, multifunctional hollow core/shell structured nanocapsules with magnetic Fe_3O_4 or Au nanocrystals as the cores, thin mesoporous silica layer as the shell and controllable cavities between the core and shell have been fabricated and applied as both MRI contrast agent and carriers for anticancer DDSs. We employed the magnetite core-based nanocapsules of ellipsoidal morphology to demonstrate our concept of multifunctional core/shell nanocapsules as DDSs because mesoporous nanomaterials with larger aspect ratios could be taken up by cells in larger amounts and have higher internalization rates,[40,41] which is of great significance for the enhancement of chemotherapy effectiveness. Besides, the reason for adopting magnetic Fe_3O_4 nanocrystals to functionalize the nanocapsules is that magnetic nanocrystals could be used for magnetically targeted drug delivery,[4,42] magnetic hyperthermia,[43] and as MRI contrast agents as well.[44,45] This is the first report, as far as we know, to prepare multifunctional core/shell structured hollow mesoporous silica nanocapsules with ellipsoidal morphology as both MRI imaging agents and DDSs. Moreover, the concept of multifunctional inorganic nanocapsules was extended to design and prepare Gd−Si−DTPA grafted Au@mSiO_2 nanocapsules for T_1-weighted MRI and dark-field light scattering live cell imaging, further demonstrating the generality of this strategy for the preparation of multifunctional mesoporous nanocapsules.

RESULTS AND DISCUSSION

Synthesis of Core/Shell Structured Multifunctional Hollow Mesoporous Nanocapsules. As shown in Scheme 1, monodispersed ellipsoidal Fe_2O_3 nanocrystals were chosen as the morphology-deciding template to obtain magnetic mesoporous nanocapsules, which were fabricated by hydrothermal synthesis using iron perchlorate as the Fe precursor (Figure 1a).[4] A thick layer of dense silica was deposited onto the surface of Fe_2O_3 to form Fe_2O_3@SiO_2 core/shell nanostructures by the well-known Stöber method (Figure 1b).[46] Then, a thin layer of mesoporous silica shell could be deposited onto the surface of Fe_2O_3@SiO_2 to form a trilayered composite nanostructure (Fe_2O_3@SiO_2@mSiO_2) by the co-condensation of tetraethyl orthosilicate (TEOS) and octadecyltrimethoxysilane (C_{18}TMS) in virtue of the existence of similar -OR (R = CH_3 or C_2H_5) groups in both molecules (Figure 1c). The condensation degree between the middle dense silica layer and outer mesoporous silica layer is different, resulting in the unexpected differentiated dissolution behaviors between two silica layers. The middle silica layer (lower condensation degree) could be etched away under alkaline conditions (e.g., ammonia solution), forming huge cavities between the shell and core (Fe_2O_3@mSiO_2), while the mesoporous silica shell part (higher condensation degree) could be kept integrated.[4] Finally, the Fe_2O_3 core of the nanocapsules was reduced in a flowing gas mixture of H_2 and N_2 to produce hollow Fe_3O_4@mSiO_2 nanocapsules (Figure 2). TEM image of hollow Fe_3O_4@mSiO_2 (Figure 1d) reveals that the middle silica layer could be completely removed by alkaline etching, which is different from the ring-shaped cavity formation under hydrothermal treatment of spherical Fe_3O_4@SiO_2@mSiO_2 composite nanostructures caused by further condensation/densification of the middle silica layer reported by us recently.[23] It is necessary to point out that the overall diameter and morphology of the composite nanocapsules, and the thickness of the outer mesoporous silica shell remain almost unchanged after the etching process, leaving a complete and huge cavity in between the thin mesopo-

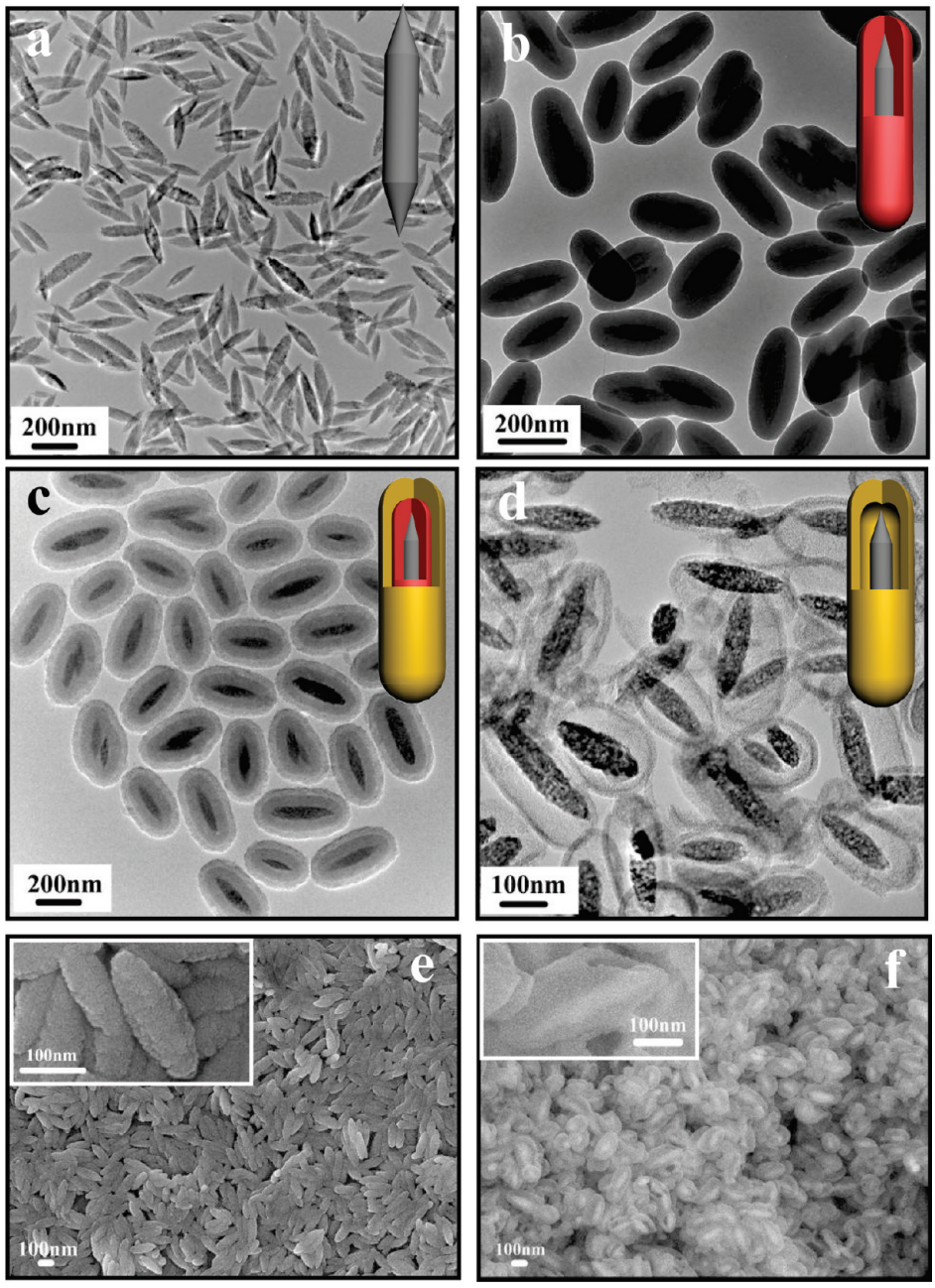

Figure 1. TEM images of ellipsoidal (a) Fe_2O_3, (b) Fe_2O_3@SiO_2, (c) Fe_2O_3@SiO_2@mSiO_2 and (d) Fe_3O_4@mSiO_2; Secondary electron SEM image of ellipsoidal Fe_2O_3 (e, inset: SEM image at high magnification) and backscattered electron SEM (f) image of ellipsoidal Fe_3O_4@mSiO_2 nanocapsules (inset: purposely selected backscattered electron image of broken nanocapsules to reveal the hollow nanostructure).

rous shell and magnetic Fe_3O_4 core. In addition, the dimension of the cavity in Fe_3O_4@mSiO_2 nanocapsules could be simply tuned by selecting adequate etching time, supported by TEM observations of different etching time intervals (Figure 3; 0 h, 4 h, 12 and 24 h) of Fe_2O_3@SiO_2@mSiO_2 composite nanostructures. A secondary electron SEM image of the Fe_2O_3 nanocrystals and Fe_3O_4@mSiO_2 show that the particles are uniformly ellipsoidal in shape (Figure 1e and 1f), while a compositional backscattered SEM image (Figure 1f) reveals the contrast difference between the central heavy core and the cavity/silica shell of the hollow structure, which could be further confirmed by a purposely selected broken nanocapsule (inset of Figure 1f).

N_2 adsorption−desorption technique was adopted to characterize the pore structural evolution of the magnetic nanocapsules after alkaline etching in ammonia solution. Surprisingly, the isotherms of Fe_3O_4@SiO_2@mSiO_2 core/shell nanostructures and Fe_3O_4@mSiO_2 nanocapsules show apparently different styles, where rattle-type core−shell nanocapsules exhibit a much larger hysteresis loop than those without

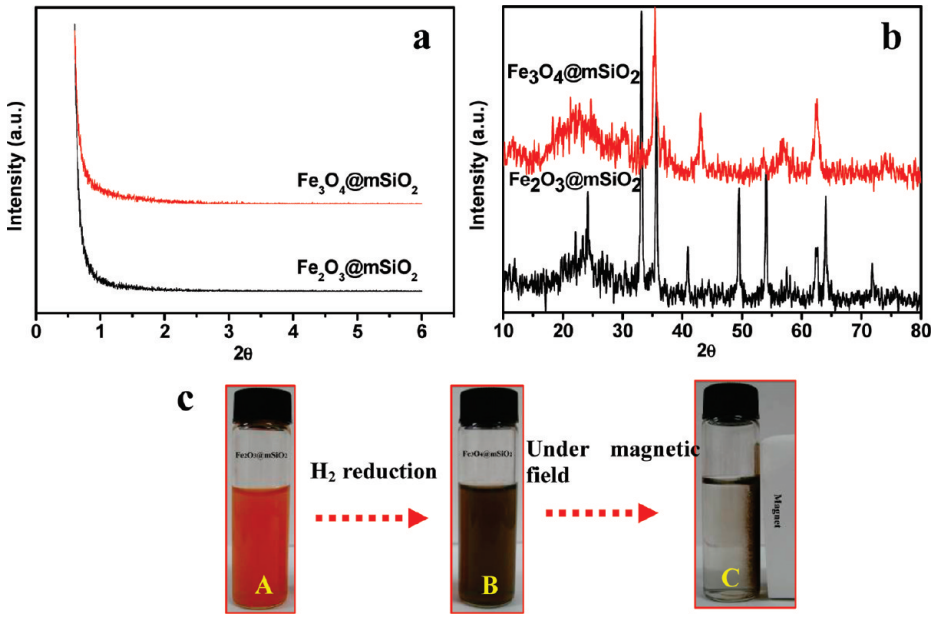

Figure 2. (a) Small-angle and (b) wide-angle X-ray diffraction patterns of Fe_2O_3@mSiO$_2$ and Fe_3O_4@mSiO$_2$ nanocapsules. (c) Digital pictures of (A) Fe_2O_3@mSiO$_2$ and (B) Fe_3O_4@mSiO$_2$ dispersed in PBS solution, and (C) Fe_3O_4@mSiO$_2$ nanocapsules in PBS solution under magnetic field. The appearance of characteristic diffraction peaks in wide-angle XRD pattern of Fe_3O_4 in Fe_3O_4@mSiO$_2$ and disappearance of characteristic diffraction peaks of Fe_2O_3 in Fe_2O_3@mSiO$_2$ demonstrated the successful conversion of Fe_2O_3@mSiO$_2$ into Fe_3O_4@mSiO$_2$. Besides, small-angle XRD patterns indicated that the mesopores in the nanocapsules are disordered, in consistent with TEM observations.

cavities between the core and shell (Figure 4a), which represents the typical ink-bottle-type pores in which larger cavities are connected by narrow windows.[47] The surface area increased from 261 m^2/g to 318 m^2/g while the pore volume from 0.44 cm^3/g to 0.78 cm^3/g after alkaline etching. The average pore size of Fe_3O_4@mSiO$_2$ also increased from 2.5 to 3.6 nm (Figure 4b). As shown in Scheme 2, the mesoporous silica shell of Fe_2O_3@SiO$_2$@mSiO$_2$ is still relatively unstable under alkaline condition because of the existence of abundant Si−O−Si bonds in the shell.[4,48] Partial Si−O−Si bonds in the shell can be broken during the etching process, resulting in the enlargement of the initial pores templated by the surfactants (C_{18}TMS) and finally causing the increase of surface area and pore volume. According to above analysis, we believe that this etching process provides an alternative but versatile route to tune the structural parameter of mesoporous nanocapsules, such as surface area, pore volume and pore size. Selective etching of silica to form nanocapsules, such as Au@SiO$_2$, CNTs@SiO$_2$[49] and SiO$_2$@SiO$_2$,[50] has been reported recently. However, there were no well-defined mesoporous structures on those silica shells due to their intrinsic absence, which may limit their practical applications due to the mass transfer blockage by the solid silica shells. Our prepared Fe_3O_4@mSiO$_2$ hollow core/shell nanocapsules with well-defined mesopores in the silica shell and controllable cavity sizes show the apparent advantage superior to nonporous inorganic nanocapsules in drug delivery and/or magnetic-recycled catalysis applications.

Cell Uptake, Intracellular Location, Cytotoxicity, Hemolysis, Coagulation of Multifunctional Mesoporous Fe_3O_4@mSiO$_2$ Nanocapsules. Excellent cell uptake of the prepared inorganic nanocapsules guarantees the high delivery efficiency of encapsulated drugs because intracellular release of drugs from the carriers could cause higher cytotoxicity than extracellular drugs. To facilitate the observations of cell uptake of the nanocapsules by confocal laser scanning microscopy (CLSM), the prepared Fe_3O_4@mSiO$_2$ nanocapsules were grafted by fluorescein isothiocyanate (FITC-capsules). Figure 5a$_1$−a$_3$ show bright-field, fluorescent and merged images of breast cancer MCF-7 cells incubated with FITC-capsules (100 μg/mL) for 3 h. The CLSM images show that the nanocapsules could be taken up by MCF-7 cells within a short period as manifested by the appearance of green fluorescence in cells. The overlay of the bright field and fluorescent images further demonstrate that the luminescence is strongly correlated with the intracellular location (Figure 5a and S1, Supporting Information), suggesting the feasibility and efficiency of the nanocapsules for fluorescent cell imaging and anticancer drugs delivery into cancer cells. To further reveal the uptake mechanism of the magnetic nanocapsules into MCF-7 cells and the intracellular location, bio-TEM analysis was carried out after ultrathin section of MCF-7 cells after the uptake of the nanocapsules. The distribution of magnetic nanocapsules could be clearly observed in TEM images, and a large number of them were found in the cytoplasm while no nanocarriers were found in the nucleus (Figure 5b$_1$ and b$_2$). In addition, part of the nanocapsules could be found near the cell membrane forming vesicles (Figure 5b$_3$). After the uptake by cancer cells *via* endocytosis, the nanocapsules will be processed in endosomes and lysosomes, and are eventually released into the cytoplasm.[51−53]

It is important to investigate the biocompatibility of the hollow Fe_3O_4@mSiO$_2$ nanocapsules with blood cells to guarantee the successful intravenous administration of drug-loaded nanocapsules. In fact, the blood compatibility of the inorganic hollow core/shell nanocapsules has been rarely reported. Hemolysis experiment

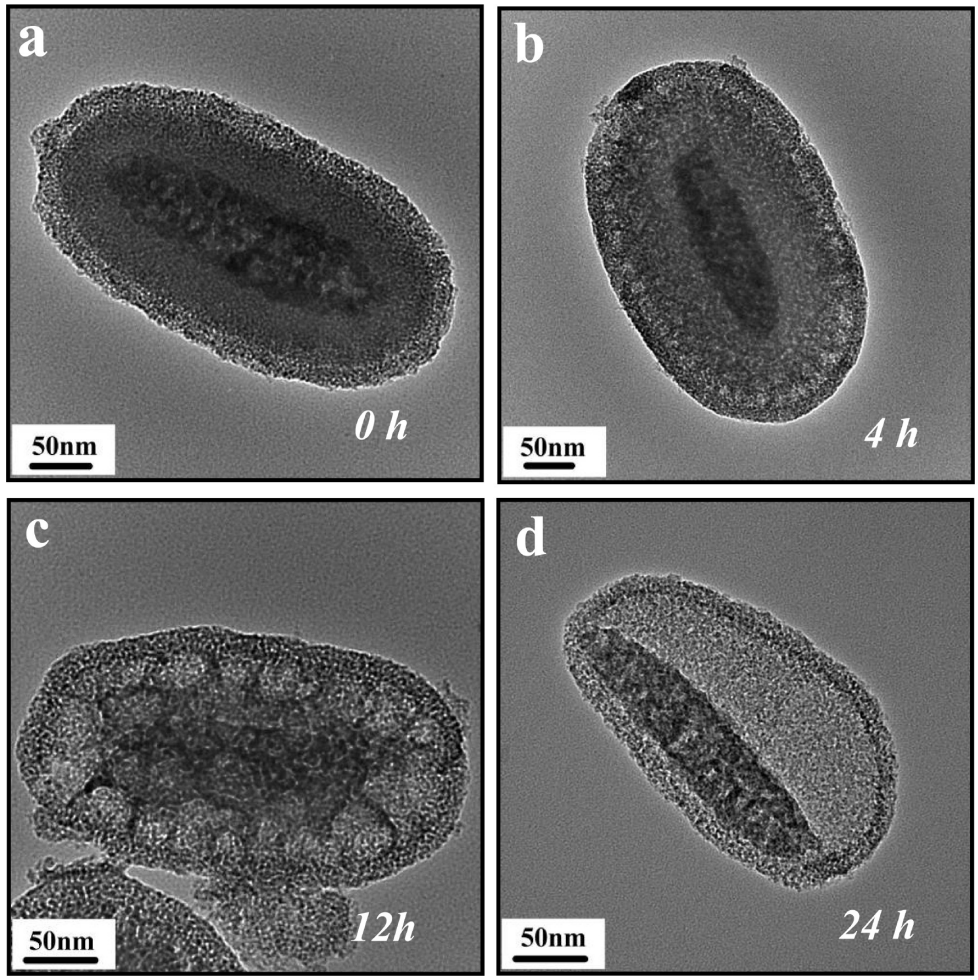

Figure 3. TEM images of magnetic mesoporous composites obtained by etching in an ammonium solution for (a) 0 h, (b) 4 h, (c) 12 h and (d) 24 h.

of the hollow Fe_3O_4@$mSiO_2$ nanocapsules was carried out preliminarily according to the previous reports about the evaluation of blood compatibility of mesoporous silica or mesoporous carbon.[4,54,55] The suspensions of red blood cells (RBCs) were isolated from freshly obtained human volunteer's blood by centrifugation and purified by successive washes with sterile isotonic phosphate saline-buffered solution (PBS) for hemolysis assay. The hemolysis results show that almost no hemolysis of RBCs could be detected in the samples of Fe_3O_4@$mSiO_2$ nanocapsules at concentrations ranging in 25−100 μg/mL, as shown in Figure 6a and S2 (Supporting Information). About 1.2 and 3.7% of hemolytic activities were distinguished at very high concentrations of 300 and 500 μg/mL, respectively, much smaller than those of traditional amorphous silica (44% of 100 μg/mL[55]), demonstrating the excellent blood compatibility of Fe_3O_4@$mSiO_2$ nanocapsules.

To evaluate the coagulation effect caused by the Fe_3O_4@$mSiO_2$ nanocapsules, prothrombin time (PT)

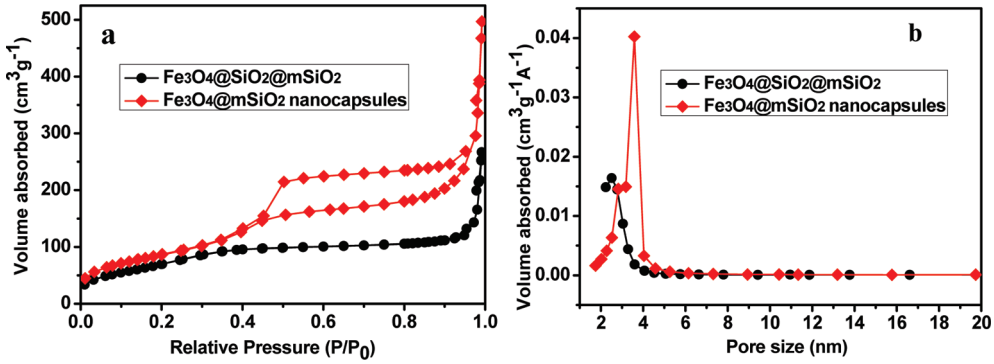

Figure 4. (a) N_2 adsorption−desorption isotherms and (b) corresponding pore diameter distributions of Fe_3O_4@SiO_2@$mSiO_2$ and Fe_3O_4@$mSiO_2$ nanocapsules after 24 h etching.

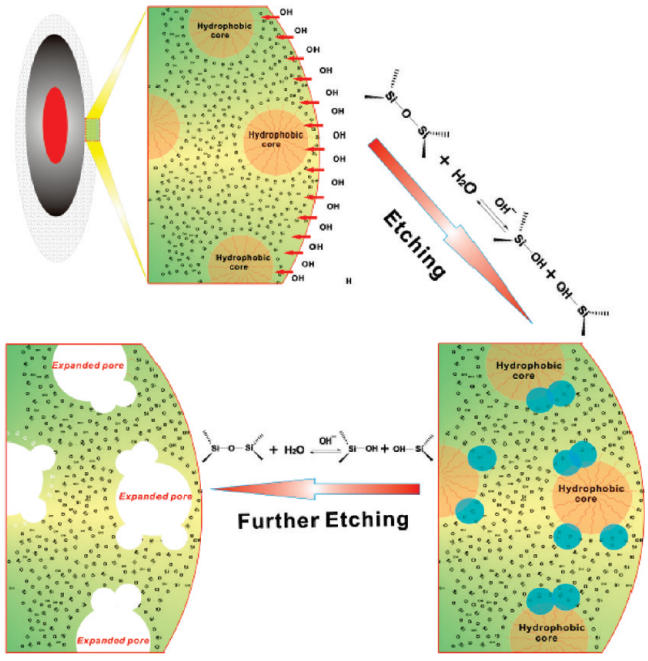

Scheme 2. Schematic Representation of the Microstructure Evolution Before, During and After the Alkaline Etching[a] [a]Si−O−Si bonds in the mesoporous silica shell part could be partially broken by OH^{-1} in ammonia solution under hydrothermal treatment (150°C; 24 h), causing the expansion of sizes of initial pores templated by C_{18}TMS.

and activated partial thromboplastin time (APTT) values were tested by mixing fresh blood plasma with nanocapsules at different concentrations (25−500 μg/mL). As shown in Figure S3 (Supporting Information), the PT and APTT values of the plasma exposure to Fe_3O_4@mSiO_2 nanocapsules of different concentrations do not show significant difference compared to those of the blank control, demonstrating that no significant coagulation/anticoagulation effect of prepared nanocapsules is present. It is known the coagulation effect caused by the nanomaterials as DDSs in blood vessel must avoided, so the coagulation test results of Fe_3O_4@mSiO_2 nanocapsules guarantee the biosafety for the intravenous administration of the prepared nanocapsules.

To evaluate the cytotoxicity of the empty capsules, *in vitro* cytotoxicity tests were conducted against different cell lines, such as MCF-7 cells, HeLa cells and L929 cells by conducting MTT (3-[4,5-dimethylthiazol-2-yl]-2,5-diphenyltetrazolium bromide) assays. Figure 6b and S4 (Supporting Information) show the effect of concentration of Fe_3O_4@mSiO_2 nanocapsules on the cell viability for different incubation time periods. The difference in cell viabilities after 24 and 48 h of incubation is negligibly small, and there is no apparent cytotoxicity after incubation at a very high concentration up to 400 μg/mL for 48 h. The excellent biocompatibility (blood-compatibility and low cytotoxicity) of the Fe_3O_4@mSiO_2 nanocapsules guarantees the practical applications for human beings as carriers in DDSs.

Multifunctional Mesoporous Nanocapsules as Contrast Agents of MRI Both *In Vitro* and *In Vivo*. The functional inorganic nanocrystals in the core part of the nanocapsules could endow the capsules with simultaneous imaging and drug delivery functionalities. For instance, the magnetic Fe_3O_4 core of the prepared core/shell nanocapsules could be used as the MRI contrast agent during the chemotherapeutic process, playing a role of monitoring the therapeutic efficiency and providing high-quality images for operators. As an initial step in exploring potential imaging functionality of the nanocapsules during chemotherapy both *in vitro* and *in vivo*, the visibility of the nanocapsules was tested in water, in cells and in mice by MRI. T_2 phantom images of the nanocapsules dispersed in water changed significantly in signal intensity with the increase of Fe concentration (Figure S5a, Supporting Information), indicating that the magnetic nanocapsules have generated magnetic resonance contrast on transverse (T_2) proton relaxations-times weighted sequence due to the dipolar interaction of magnetic moments between the nanocapsules and proton in the water.[56,57] An r_2 value of 137.8 $mM^{-1}s^{-1}$ was measured for the magnetic nanocapsules (Figure S5b, Supporting Information), revealing high potential of the nanocapsules as T_2 contrast agents for cancer diagnosis. Under T_2-weighted imaging mode, cells exposed to the magnetic nanocapsules of a concentration of 50 μg/mL for 6 h could be easily detected (Figure S5c, Supporting Information).

Furthermore, the nanocapsules were injected into mice subcutaneously and noninvasively detected with MRI at diverse concentrations and different time intervals (Figure 5c and d). The darkened images from the injection site confirmed the imaging capability of the nanocapsules (Figure 5c, red circled area). The darkened area extended through the tumor part with time (from 1 to 24 h), indicating the diffusion of magnetic nanocapsules within tumor. Besides, the darkened area was also larger at increased concentrations, demonstrating the concentration-dependent MRI feature of magnetic nanocapsules (Figure 5d).

Multifunctional Mesoporous Nanocapsules as DDSs for Doxorubicin. To achieve the goal of complete eradication of tumors, therapeutic agents have to be administrated systematically in high dose to ensure the sufficient and sustained therapy efficiency. However, most of anticancer drugs effective in eradicating cancer cells could cause severe side-effect when the high doses are administrated, which is caused by the nonspecific uptake of anticancer drugs by healthy tissues/organs such as kidney, liver, bone marrow and heart. An effective way to reduce the side-effect is to encapsulate the anticancer drugs in DDSs with high loading amount and efficiency, which could largely protect the healthy organs from the toxic drugs and prevent the decomposition/denaturing of the drugs prior to reaching the targeted cells. We believe that the obtained multifunctional

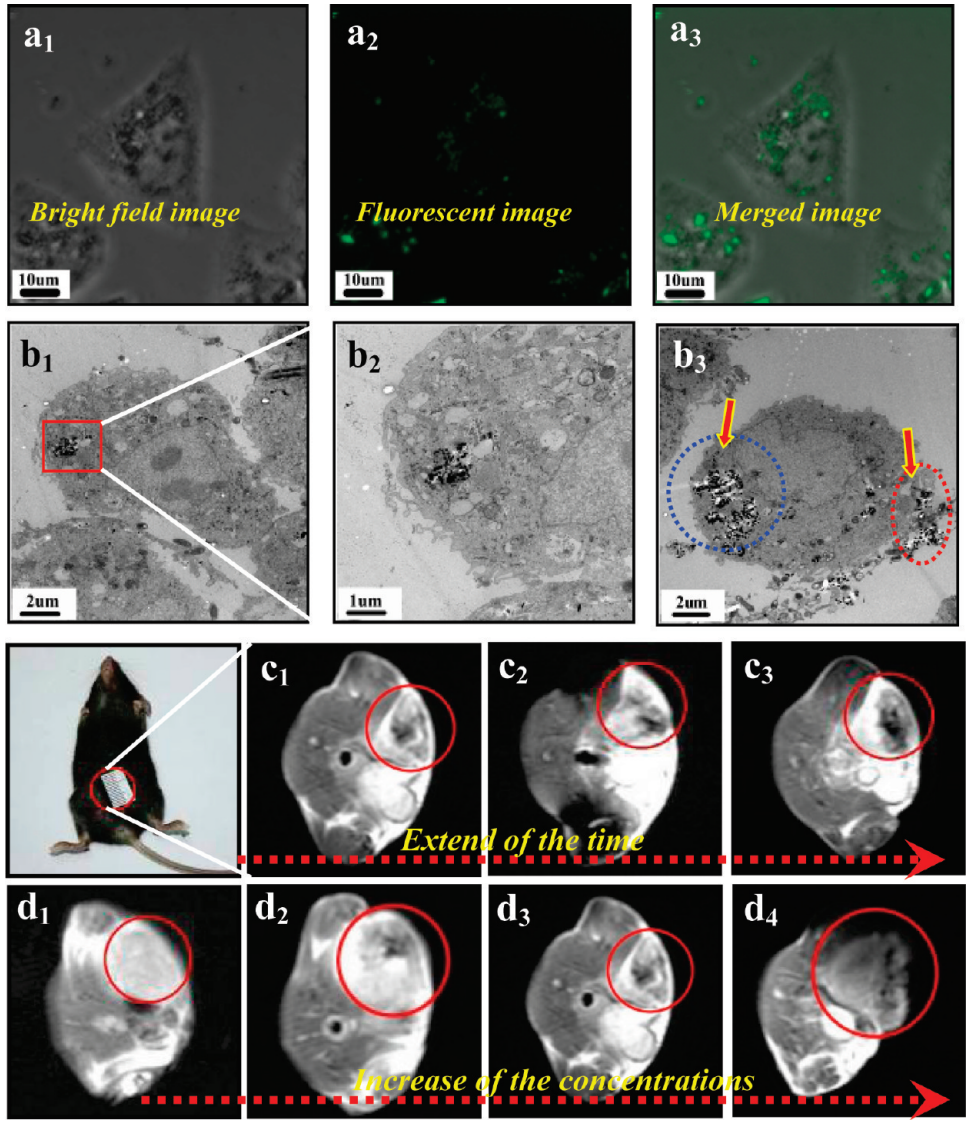

Figure 5. CLSM images (a_1-a_3) of MCF-7 cells after incubation with 100 μg/mL FITC-nanocapsules. Bio-TEM images (b_1-b_3) of MCF-7 cells after incubation with magnetic Fe_3O_4@$mSiO_2$ nanocapsules. *In vivo* MRI (c and d) of a tumor-bearing mouse before and after injection of magnetic Fe_3O_4@$mSiO_2$ nanocapsules for different time intervals (c_1, 1 h; c_2, 4 h and c_3, 24 h at 500 μg/mL of Fe_3O_4@$mSiO_2$ nanocapsules) and at different nanocapsule concentrations (d_1, control; d_2, 250 μg/mL; d_3, 500 μg/mL; d_4, 1000 μg/mL in 1 h of postinjection).

nanocapsules with huge cavities between the core and shell, and enhanced large surface area/pore volume of mesoporous shell, could be used to encapsulate anticancer drugs with high amount and efficiency. To demonstrate this hypothesis, a typical and widely used anticancer drug, doxorubicin hydrochloride (DOX), was chosen as a model drug to investigate the loading amount, encapsulation efficiency and *in vitro* interaction with cancer cells. The effective DOX storage capacities of the obtained samples immersed into a DOX/PBS (pH = 7.4) solution can be monitored by UV−vis absorbance spectrometry. Figure 6c shows the UV−vis absorbance spectra of 0.5 mg/mL DOX/PBS solutions before and after the interaction with the nanocapsules. The DOX in PBS solution could be well loaded into the magnetic nanocapsules with a high efficiency, which was demonstrated by the disappearance of the characteristic absorbance peaks in UV−vis spectrum and the color change of DOX solution after the interaction with the nanocapsules (inset of Figure 6c). The loading amount of DOX in the nanocapsules is about 20%. It is known that organic carriers, such as liposome and micelles, could store drugs with high efficiency but low loading capacity, whereas inorganic carriers, such as mesoporous silica nanoparticles, usually showed high drug loading capacity, however, the loading efficiency is usually low. Our drug delivery system with both high drug loading capacity and efficiency was attributed to the enhanced surface area/pore volume, formation of cavities to leave more room for drug molecules and the electrostatic interaction between positively charged DOX molecules and negatively charged mesoporous silica surface.[37,58] It is commonly accepted that mesoporous materials possess sustained drug release

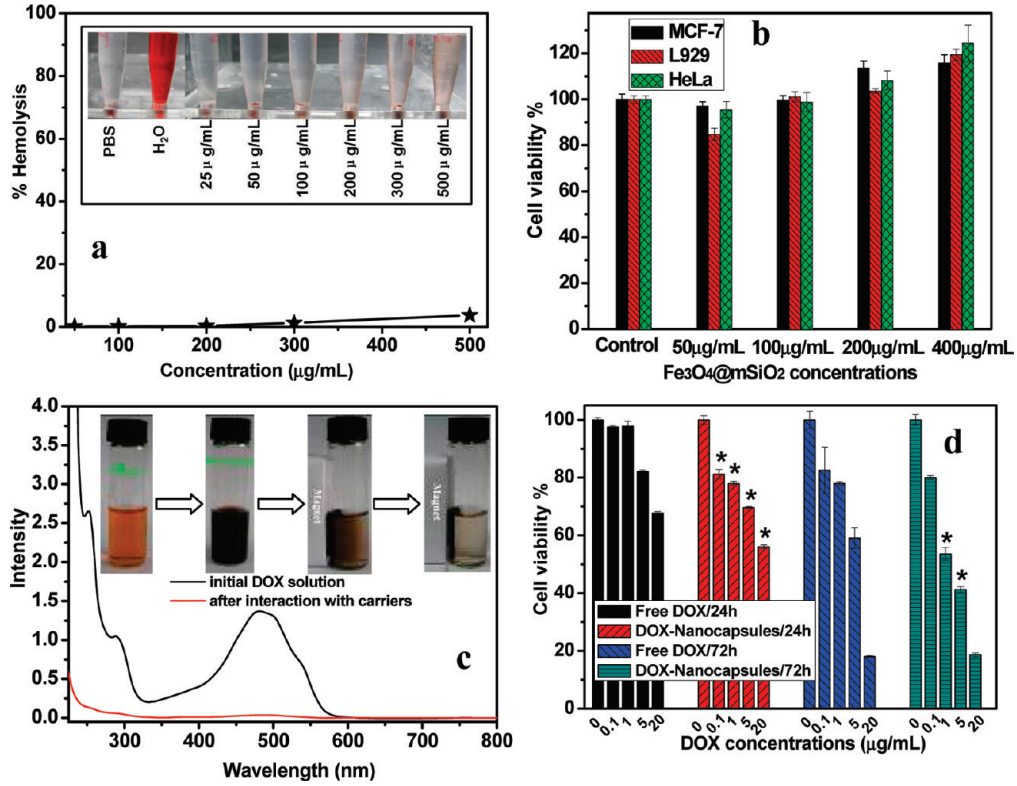

Figure 6. (a) Hemolysis assay for the magnetic nanocapsules (inset: photographic images for direct observation of hemolysis by the nanocapsules, using PBS as a negative control and water as positive control (the two tubes on the left), and the capsules suspended at different concentrations (the six tubes on the right)). The red blood cells are red due to the presence of hemoglobin in the RBCs. During the hemolysis assay experiment, hemoglobin will be released into the solution by hemolysis, resulting in visually red color in solution. (b) Cell viabilities of the empty nanocapsules against MCF-7 cells, L929 cells and HeLa cells at different concentrations for 24 h. (c) UV−vis spectra of DOX before and after interaction with the nanocapsules (inset, from left to right: digital pictures of pure DOX solution, and the nanocapsules added DOX solutions before, after 30 s magnetic field attraction and after complete magnetic field attraction). The color of DOX/PBS solution changes from the red to colorless, demonstrating the complete loading of DOX molecules into the nanocapsules. (d) Cell viabilities of free DOX and DOX loaded Fe_3O_4@$mSiO_2$ nanocapsules against MCF-7 cells at different concentrations for 24 and 72 h (*represent significance difference compared with free DOX with the same drug concentration at $P < 0.05$).

property.[59−62] Combined with this special sustained drug release property and simultaneous high loading capacity/efficiency for DOX, Fe_3O_4@$mSiO_2$ nanocapsules could be used in chemotherapy for cancer treatment with continuous therapy without frequent interval medication administrations.

To verify whether the released DOX was pharmacologically active, the cytotoxic effect of the DOX-loaded Fe_3O_4@$mSiO_2$ nanocapsules against breast cancer MCF-7 cells was tested. As shown in Figure 6d, DOX loaded Fe_3O_4@$mSiO_2$ nanocapsules induced the MCF-7 cell death comparatively to free DOX, which indicates that the loaded DOX keeps its pharmaceutical activities. The DOX loaded magnetic nanocapsules exhibited even greater cytotoxicity than free DOX after cultured for 24 and 72 h at DOX concentrations not higher than 20 μg/mL. It has been understood that the intracellular action site of DOX is within the nucleus, and delivery of DOX into cancer cells and accumulation in the nucleus can ensure its antitumor activity.[63,64] The higher DOX accumulation from Fe_3O_4@$mSiO_2$ nanocapsules in the nucleus might be partly attributed to the different cell uptake mechanism between free DOX and DOX loaded nanocapsules. For free DOX, the cell uptake mechanism is a passive diffusion process, while for DOX loaded carriers, a possible endocytosis mechanism is involved, which is more effective than the pas-

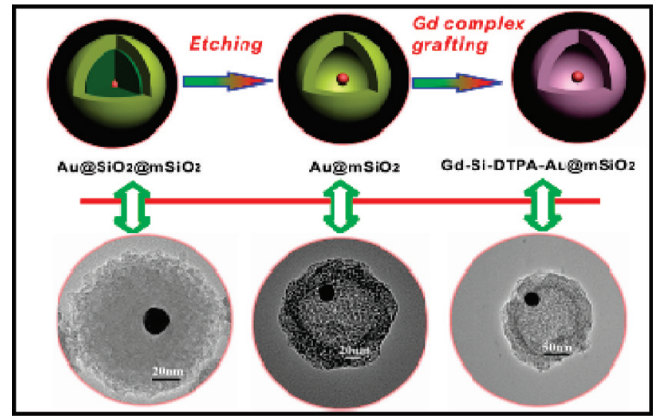

Figure 7. Schematic representation (top) and TEM images (bottom) of Au@SiO_2@$mSiO_2$, Au@$mSiO_2$ and Gd−Si−DTPA-Au@$mSiO_2$.

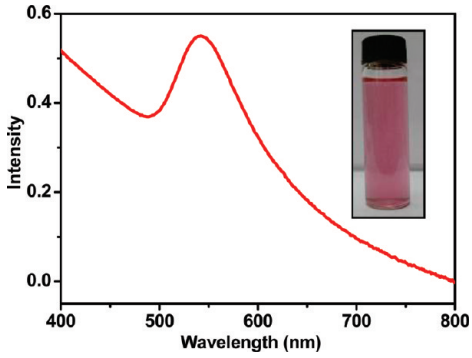

Figure 8. UV−vis spectrum of Gd−Si−DTPA-Au@mSiO$_2$ nanocapsules. (Inset) Digital picture of the solution.

sive diffusion. After incubated with MCF-7 cells, the majority of DOX-containing nanocapsules are endocytosed by the cancer cells, whereas, only limited amount of DOX diffused into the cells for free DOX. Thus, the better uptake of DOX-containing nanocapsules by the MCF-7 cells should be responsible for the higher concentration of DOX in the nucleus, leading to the enhanced DOX cytotoxicity and cell death. On the other hand, when the cancer cells are treated with free DOX, the development of multidrug resistance (MRD) of cancer cells, which results from the expression of *p*-glycoprotein pump in the cell membrane, hampers the drug action by pumping out drug molecules from cytosol to extracellular area.[65] However, the uptake of the drug loaded nanocarriers within cancer cells might, to some extent, circumvent the MRD effect.[65]

Preparation of Au@mSiO$_2$ Nanocapsules and Their Biological Bimodal Imaging. Many functional inorganic nanocrystals could be coated by silica layers. The subsequent mesoporous silica layer coating depends on the surface chemistry of coated dense silica layer rather than the nanocrystals, so this nanocapsule formation strategy could be extended to synthesize various multifunctional hollow core/shell structured nanocapsules by simply changing the functional core, depending on the practical requirements and elaborate design in nano/micrometer scale.

We further substituted ellipsoidal Fe_3O_4 with spherical Au nanoparticles to demonstrate this hypothesis, in virtue of the unique optical properties of Au nanoparticles such as surface plasma resonance enhanced light scattering and absorption, and the ability to efficiently convert the strongly absorbed light into localized heat, which could be exploited for *in vivo* imaging and the selective laser photothermal therapy of cancer.[66] Furthermore, we grafted Gd−Si−DTPA into the pores of Au@mSiO$_2$ nanocapsules using the abundant surface chemistry of mesoporous silica layer (e.g., Si−OH), which could be used for biological bimodal imaging including dark-field light scattering cell imaging and T_1-weighted MRI, and anticancer drug encapsulation and delivery. Figure 7 and S6 show the structural evolution during the preparation process, including coating nonporous silica and mesoporous silica shells on Au surface, etching away the middle silica layer and further grafting Gd−Si−DTPA (T_1 MRI contrast agent) for multifunctionalization. The obtained Gd complex grafted Au@mSiO$_2$ nanocapsules exhibit strong surface plasma enhanced absorption (Figure 8), which makes them useful for biomedical dark-field light scattering imaging and detection of live cells (Figure 9).[67] Besides, the obtained Gd−Si−DTPA grafted Au@mSiO$_2$ nanocapsules show T_1-weighted signal enhancement with a r_1 value of 7.43 $mM^{-1}s^{-1}$, demonstrating the potential application in T_1-weighted MRI (Figure 10).

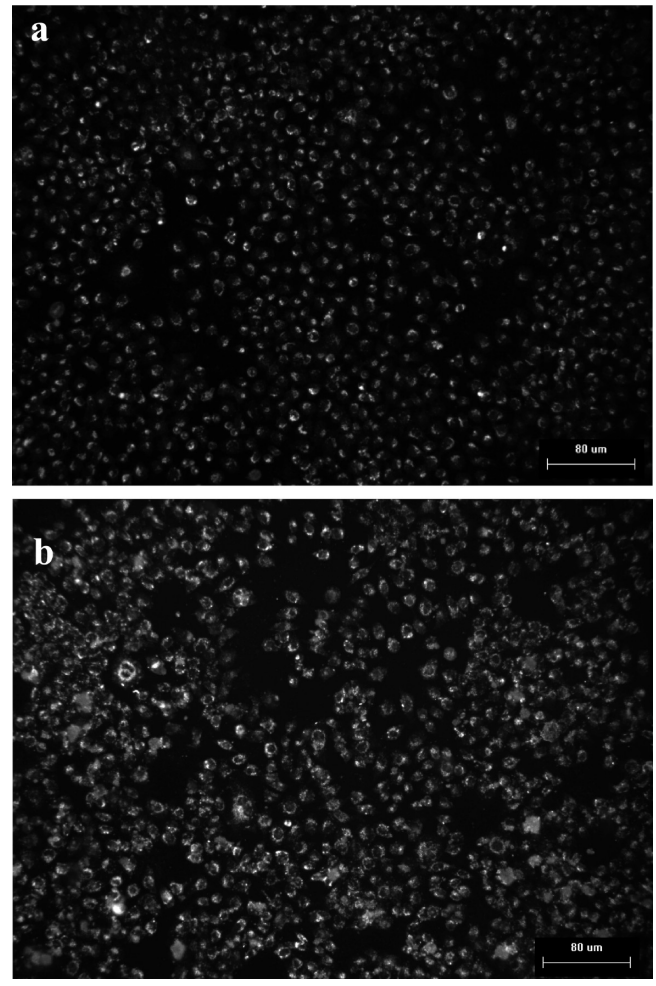

Figure 9. Dark-field optical microscopic images of HeLa cells (a) before and (b) after incubation with 100 μg/mL Gd−Si−DTPA grafted Au@mSiO$_2$ nanocapsules. Dark-field microscopic observation of Gd−Si−DTPA grafted Au@mSiO$_2$ nanocapsules was carried out to evaluate whether the obtained multifunctional nanocapsules could be used for optical cell imaging, which is endowed by the special light scattering ability of Au nanoparticles. The experimental condition for obtaining the images of HeLa cells before and after the treatment was the same. From the images, it could be seen that the HeLa cells could scatter light to a certain degree, the outline of which could not be clearly distinguished. However, HeLa cells could be lit up by Gd−Si−DTPA grafted Au@mSiO$_2$ nanocapsules, which could be directly observed from the clear cell outlines. This implies that obtained Au@mSiO$_2$ multifunctional nanocapsules could be uptaken by cells and used for optical cell imaging.

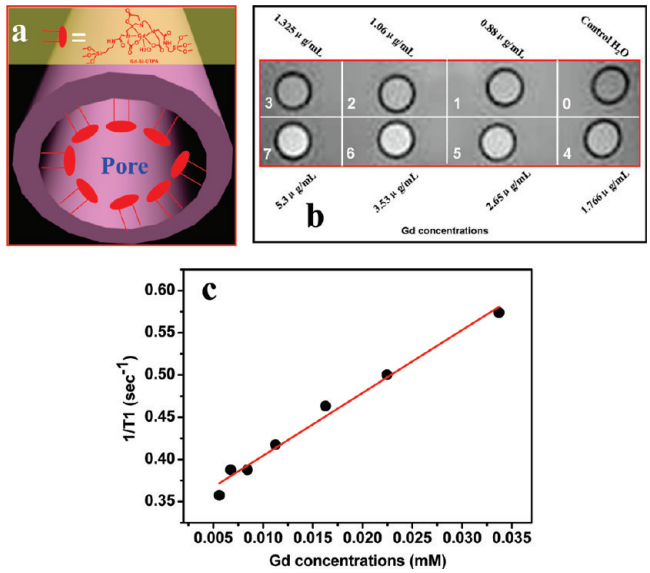

Figure 10. Schematic illustration of the Gd−Si−DTPA grafting of (a) Au@mSiO$_2$ nanocapsules and (b) T$_1$-weighted images of Gd−Si−DTPA-Au@mSiO$_2$ nanocapsules of different Gd concentrations in water; (c) r_1 relaxation curve of Gd−Si−DTPA-Au@mSiO$_2$ nanocapsules.

CONCLUSIONS

In summary, the concept of hollow core/shell structured mesoporous nanocapsules as multifunctional DDSs has been demonstrated by using ellipsoidal Fe_3O_4@mSiO$_2$ nanocapsules as an example of a promising platform for simultaneous drug delivery and cell imaging. The obtained Fe_3O_4@mSiO$_2$ nanocapsules showed much increased surface area and pore volume after the removal of the middle silica layer from Fe_2O_3@SiO$_2$@mSiO$_2$ nanostructures for middle cavity formation, and the cavity space between the core and shell, together with the pore size on the thin mesoporous silica shell could be well controlled by changing experimental conditions of the selective etching process. Importantly, the Fe_3O_4@mSiO$_2$ nanocapsules showed high loading capacity (20%) and encapsulation efficiency (up to 100%) for doxorubicin simultaneously. The excellent biocompatibility of Fe_3O_4@mSiO$_2$ was demonstrated by its negligible hemolysis against human blood cells, no significant coagulation effect against human blood plasma and very low cytotoxicity against various cell lines (MCF-7, HeLa and L929). The cytotoxicity of doxorubicin loaded Fe_3O_4@mSiO$_2$ against human breast cancer MCF-7 cells was higher than free doxorubicin at relatively low drug concentrations because of the intracellular release of drugs and reduced MRD effect. Besides, the potential application of Fe_3O_4@mSiO$_2$ nanocapsules as contrast agents for MRI was also demonstrated both *in vitro* and *in vivo*. The results indicate that biocompatible magnetic Fe_3O_4@mSiO$_2$ nanocapsules are the excellent anticancer drug carriers for the simultaneous imaging diagnosis and chemotherapy applications. In addition, various types of multifunctional platforms of core/shell structured mesoporous nanocapsules could be obtained by using the similar synthetic strategy but different inorganic cores, such as Gd−Si−DTPA grafted Au@mSiO$_2$ nanocapsules, which was also demonstrated and discussed in this paper.

EXPERIMENTAL METHODS

Materials. Tetraethyl orthosilicate (TEOS), ethanol, ammonia solution (25−28%), urea, pyridine, sodium citrate tribasic dehydrate, $HAuCl_4 \cdot 3H_2O$ and NaH_2PO_4 were obtained from Sinopharm Chemical Reagent Co.. Octadecyltrimethoxysilane (C_{18}TMS) was purchased from Tokyo Chemical Industry Co., Ltd.. PBS solution (pH = 7.4) was obtained from Shanghai Runcheng Biomedical Co., Ltd.. 3-Aminopropyltriethoxysilane (APTES), $Fe(ClO_4)_3 \cdot 6H_2O$, polyvinylpyrrolidone (PVP10), diethylenetriamine pentaacetic dianhydride, fluorescein isothiocyanate (FITC) and $GdCl_3 \cdot 6H_2O$ were purchased from Sigma-Aldrich. Anticancer drug doxorubicin hydrochloride (DOX, for injection use) was provided by Zhejiang Haizheng Pharmacy Co., Ltd. Deionized water was used in all experiments.

Methods. ***Preparation of Fe_3O_4@mSiO$_2$ Nanocapsules.*** The Fe_3O_4@mSiO$_2$ nanocapsules with ellipsoidal morphology were fabricated according to a structural difference based selective etching strategy. Briefly, 30 mg of ellipsoidal Fe_2O_3 were dispersed in a mixture of 71.4 mL of ethanol, 10 mL of H_2O and 3.14 mL of ammonia solution under ultrasonic treatment. Then, 0.53 mL of TEOS was diluted in 4 mL of ethanol and added into above solution by an injection pump with the speed of 4 mL/h under magnetic stirring at room temperature. After the injection, the reaction solution was stirred for another 1 h (Fe_2O_3@SiO$_2$). A mixture of 0.3 mL of TEOS, 0.2 mL of C_{18}TMS and 4 mL of ethanol was injected into the reaction medium by the injection pump at the speed of 4 mL/h, and then the reaction was continued for another 1 h at room temperature by magnetic stirring (Fe_2O_3@SiO$_2$@mSiO$_2$). The product was collected by centrifugation with the speed of 10 000 rmp for 10 min. Half the product was then dispersed in 50 mL of H_2O by ultrasonic treatment for 2 h. Then, 7 mL of ammonia solution (2 mol/L) was added into the solution, which was put in an autoclave (100 mL volume) and transferred into the baking oven (150 °C) for different time intervals (Fe_2O_3@mSiO$_2$). After the autoclave was cooled down to room temperature, the sample was collected and washed with H_2O and ethanol for several times. Then the sample was dried at 100 °C and calcined at 550 °C for 10 h to burn out the surfactant (C_{18}TMS). Finally, to transform Fe_2O_3@mSiO$_2$ nanocapsules into magnetic Fe_3O_4@mSiO$_2$ nanocapsules, the sample was reduced in a mixed H_2 (5% volume percentage) and Ar (95% volume percentage) gases at 410 °C for 5 h.

Hemolysis Assay. The hemolysis assay experiments were carried out according to previous reports.[4,54,55] To be further close to the actual situation, human blood stabilized by EDTA, which was kindly provided by Shanghai Blood Center (obtained from volunteers), was employed to evaluate the blood compatibility of obtained nanocapsules. The red blood cells (RBCs) were collected by removing the serum from the blood by centrifugation and suction. The RBCs were purified by washing with PBS for five times. Then, the RBCs were diluted to 1/10 of their initial volume with PBS solution. A 0.3 mL suspension of diluted RBCs suspension was then mixed with: a) 1.2 mL of PBS as a negative control; b) 1.2 mL of deionized water as a positive control; c) 1.2 mL of magnetic nanocapsules suspensions (PBS) at concentrations ranging from 25 to 500 μg/mL. The mixtures were then shook and stood still for 2 h at room temperature. The samples were centrifuged and the absorbance of the supernatants at 541 nm was measured by a UV−vis spectroscope.

In Vitro Cytotoxicity. *In vitro* cytotoxicity of magnetic Fe_3O_4@$mSiO_2$ nanocapsules was assayed against different cell lines, including breast cancer MCF-7 cells, cervical HeLa cells and mouse fibroblast L929 cells. Cells (MCF-7, HeLa and L929) were seeded in a 96-well plate at a density of 10^4 cells per well and cultured in 5% CO_2 at 37 °C for 24 h. Then, the nanocapsules were added to the medium separately, and then the cells were incubated in 5% CO_2 at 37 °C for 24 and 48 h. The concentrations of the nanocapsules were 50, 100, 200, 400 μg/mL respectively. At the end of the incubation, the media containing the nanocapsules was removed, and 100 μL of 3-[4,5-dimethylthiazol-2-yl]-2,5-diphenyltetrazolium bromide (MTT) solution (diluted in a culture media with a final concentration of 0.8 mg/mL) was added and incubated for another 4 h. The medium was then replaced with 100 μL of dimethyl sulfoxide (DMSO) per well, and the absorbance was monitored using a microplate reader (Bio-Tek ELx800) at the wavelength of 490 nm. The cytotoxicity was expressed as the percentage of cell viability compared to untreated control cells.

Cell Internalization of Fe_3O_4@$mSiO_2$ Nanocapsules for Confocal Laser Scanning Microscopy (CLSM) Observations. Fluorescein isothiocyanate (FITC) was grafted into the nanocapsules to facilitate CLSM observations, which was described as follows: FITC (15 mg) was reacted with 3-aminopropyltriethoxysilane (APTES, 100 μL) in ethanol (5 mL) under dark conditions for 24 h. Subsequently, magnetic nanocapsules (20 mg) were reacted with FITC-APTES stock solution (1 mL) under dark conditions for 24 h. The FITC grafted nanocapsules were collected by centrifugation and washed with ethanol several times to remove the unreacted FITC-APTES. Finally, the FITC-nanocapsules were dried under vacuum at room temperature. For CLSM observations, MCF-7 cells were seeded in a 6-well plate with one piece of cover glass at the bottom of each well in incubation medium (DMEM containing 10% FBS, 100 U/mL ampicillin, 100 μg/mL streptomycin) and incubated for 24 h at 37 °C. FITC-nanocapsules were added into the incubation medium at the concentration of 100 μg/mL for 3 h incubation in 5% CO_2 at 37 °C. After the medium was removed, the cells were washed twice with cold PBS (pH = 7.4) and the cover glass was visualized under a laser scanning confocal microscope (FluoView FV1000, Olympus).

Bio-TEM Observations. The MCF-7 cells were incubated with 200 μg/mL of magnetic nanocapsules for 24 h. Then, the cells were washed twice with D-hanks and detached by incubation with 0.25% trypsin for 5 min. The cell suspension was centrifuged at 5000 r/min for 2 min. After the removal of incubation medium, the MFC-7 cells were fixed by glutaraldehyde at room temperature, then rinsed with PB and dehydrated through a graded ethanol series, finally cleared with propylene oxide. Then, the cell sample was embedded in EPOM812 and polymerized in the oven at 37 °C for 12 h, 45 °C for 12 h and 60 °C for 48 h. Ultrathin sections of approximately 70 nm thick were cut with a diamond knife on a Leica UC6 ultramicrotome and transferred to the copper grid. The images were viewed on JEM-1230 electron microscopy.

DOX Loading, Intracellular DOX Delivery and Cytotoxicity Assay. Ten milligrams of magnetic nanocapsules were mixed with 5 mL of DOX solution in PBS (0.5 mg/mL). After stirred for 24 h under dark conditions, the DOX-loaded particles were collected by centrifugation. To evaluate the DOX loading capacity, the supernatant was collected and the residual DOX content was measured by UV−vis measurements at the wavelength of 480 nm. To test the cytotoxicity of DOX loaded magnetic Fe_3O_4@$mSiO_2$ nanocapsules, breast cancer cells MCF-7 were seeded in a 96-well plate at a density of 2×10^3 cells per well and cultured in 5% CO_2 at 37 °C for 24 h. Then, free DOX, DOX-nanocapsules were added to the medium, and the cells were incubated in 5% CO_2 at 37 °C for 24 and 72 h. The concentrations of DOX were 0.1, 1, 5, 20 μg/mL, respectively. Cell viability was determined using MTT assay, which was the same as the procedure for cytotoxicity assay for the empty Fe_2O_3@$mSiO_2$ nanocapsules.

MRI Test. The *in vitro* MR imaging experiment was performed on a 3.0 T clinical MRI instrument (GE Signa 3.0 T), and the pulse sequence used was a T_2-weighted Fast-recovery fast spin−echo (FR-FSE) sequence with the following parameters: TR = 4000 ms, slice thickness = 3.0, TE = 98 ms, echo length = 15 ms. For MRI tests, the Fe content (or Gd) of the nanocapsules in water was determined by inductively coupled plasma atomic emission spectrometry (ICP-AES). For *in vitro* MCF-7 cells MRI test, 2×10^6 of MCF-7 cells were seeded in a culture dish for 24 h. Then, the as-prepared magnetic nanocapsules were incubated with cells for 6 h at the concentration of 50 μg/mL. After washed by D-hanks for three times, the cells were detached by incubation with 0.25% trypsin for 5 min. The detached cells were collected by centrifugation at 5000 rmp for 2 min. Then the cells were imaged on a 3.0 T clinical MRI instrument (GE signa 3.0 T). For *in vivo* MRI test, C57/BL6 mice bearing melanoma tumor were selected to assay the imaging ability of the magnetic nanocapsules. *In vivo* MRI was carried out before and at selected time intervals (1 h, 4 and 24 h) after the injection of magnetic nanocapsules with the same concentrations (500 μg/mL in physiological saline solution). Moreover, magnetic Fe_3O_4@$mSiO_2$ nanocapsule physiological saline solution (250 μg/mL, 500 μg/mL and 1000 μg/mL, respectively) was subcutaneously injected right at the tumor site of the tumor-bearing mouse. Then the mouse was taken for the T_2-weighted MRI test. Animal procedures were in agreement with the guidelines of the Instituonal Animal Care and Use Committee.

Dark-Field Microscopy Observations of HeLa Cells Before and After Incubation with Gd−Si−DTPA Grafted Au@$mSiO_2$ Nanocapsules. HeLa cells were seed in culture dishes until the cell density reached about 80%. The obtained Gd−Si−DTPA grafted Au@$mSiO_2$ nanocapsules were dispersed into culture medium (DMEM containing 10% FBS, 100 U/mL ampicillin, 100 μg/mL streptomycin) at the concentration of 100 μg/mL by ultrasonic treatment. Then, cell culture containing multifunctional nanocapsules was added into the culture dish, which was incubated with HeLa cells for 12 h. After the incubation, the cells were washed with D-hanks for three times to remove the nanocapsules which were not uptaken by HeLa cells. HeLa cells without incubation with nanocapsules were used as control. The dark field microscopic images were obtained on Olympus BX51 optical microscopy, using a dark-field imaging accessory.

Characterization. Transmission electron microscopy (TEM) images were obtained on a JEM-2100F electron microscope operating at 200 kV. Scanning electron microscopy (SEM) images were obtained on a field emission JEOL JSM-6700F microscope. UV−vis spectra were recorded on a UV-3101PC Shimadzu spectroscope. Nitrogen adsorption−desorption isotherms at 77K were measured on a Micrometitics Tristar 3000 system. All samples were pretreated for 12 h at 393K under nitrogen before measurements, The pore size distributions were calculated from desorption branches of isotherms by the Barrett−Joyner−Halenda (BJH) method. Pore volume and specific surface area were calculated by using Barrett−Joyner−Halenda (BJH) and Langmuir methods, respectively.

Acknowledgment. This work was supported by National Basic Research Program of China (973 Program, Grant No. 2011CB707905), National Nature Science Foundation of China (Grant No. 50823007, 51072212, 50972154), National 863 High-Tech Program (Grant No. 2007AA03Z317), Shanghai Rising-Star Program (10QH1402800), China Postdoctoral Science Foundation (20090450740) and CASKJCX Projects (Grant No. KJCX2-YW-M02, KJCX2-YW-210).

Supporting Information Available: Detailed preparation of ellipsoidal Fe_2O_3, Gd−Si−DTPA grafted Au@$mSiO_2$ nanocapsules, CLSM images, MTT assay results, hemolysis assay results, MRI test results of Fe_3O_4@$mSiO_2$, TEM images of Au@SiO_2@$mSiO_2$, Au@$mSiO_2$ and Gd−Si−DTPA-Au@$mSiO_2$, and SEM image of Gd−Si−DTPA-Au@$mSiO_2$. This material is available free of charge *via* the Internet at http://pubs.acs.org.

REFERENCES AND NOTES

1. Wang, Y. J.; Bansal, V.; Zelikin, A. N.; Caruso, F. Templated Synthesis of Single-Component Polymer Capsules and Their Application in Drug Delivery. *Nano Lett.* **2008**, *8*, 1741–1745.

2. Meier, W. Polymer Nanocapsules. *Chem. Soc. Rev.* **2000**, *29*, 295–303.
3. Qiu, X. P.; Leporatti, S.; Donath, E.; Mohwald, H. Studies on the Drug Release Properties of Polysaccharide Multilayers Encapsulated Ibuprofen Microparticles. *Langmuir* **2001**, *17*, 5375–5380.
4. Chen, Y.; Chen, H. R.; Guo, L. M.; He, Q. J.; Chen, F.; Zhou, J.; Feng, J. W.; Shi, J. L. Hollow/Rattle-Type Mesoporous Nanostructures by a Structural Difference-Based Selective Etching Strategy. *ACS Nano* **2010**, *4*, 529–539.
5. Zhang, T. R.; Ge, J. P.; Hu, Y. X.; Zhang, Q.; Aloni, S.; Yin, Y. D. Formation of Hollow Silica Colloids Through a Spontaneous Dissolution-Regrowth Process. *Angew. Chem. Int. Et.* **2008**, *47*, 5806–5811.
6. Zhu, Y. F.; Shi, J. L.; Shen, W. H.; Dong, X. P.; Feng, J. W.; Ruan, M. L.; Li, Y. S. Stimuli-Responsive Controlled Drug Release from a Hollow Mesoporous Silica Sphere/Polyelectrolyte Multilayer Core-Shell Structure. *Angew. Chem.Int. Ed.* **2005**, *44*, 5083–5087.
7. Caruso, F.; Caruso, R. A.; Mohwald, H. Nanoengineering of Inorganic and Hybrid Hollow Spheres by Colloidal Templating. *Science* **1998**, *282*, 1111–1114.
8. Donath, E.; Sukhorukov, G. B.; Caruso, F.; Davis, S. A.; Mohwald, H. Novel Hollow Polymer Shells by Colloid-Templated Assembly of Polyelectrolytes. *Angew. Chem., Int. Ed.* **1998**, *37*, 2202–2205.
9. Johnston, A. P. R.; Cortez, C.; Angelatos, A. S.; Caruso, F. Layer-by-Layer Engineered Capsules and Their Applications. *Curr. Opin. Colloid Interface Sci.* **2006**, *11*, 203–209.
10. Schneider, G.; Decher, G. From Functional Core/Shell Nanoparticles Prepared *via* Layer-by-Layer Deposition to Empty Nanospheres. *Nano Lett.* **2004**, *4*, 1833–1839.
11. Wang, Y.; Angelatos, A. S.; Caruso, F. Template Synthesis of Nanostructured Materials *via* Layer-by-Layer Assembly. *Chem. Mater.* **2008**, *20*, 848–858.
12. Pastoriza-Santos, I.; Scholer, B.; Caruso, F. Core-Shell Colloids and Hollow Polyelectrolyte Capsules Based on Diazoresins. *Adv. Funct. Mater.* **2001**, *11*, 122–128.
13. Yu, J.; Javier, D.; Yaseen, M. A.; Nitin, N.; Richards-Kortum, R.; Anvari, B.; Wong, M. S. Self-Assembly Synthesis, Tumor Cell Targeting, and Photothermal Capabilities of Antibody-Coated Indocyanine Green Nanocapsules. *J. Am. Chem. Soc.* **2010**, *132*, 1929–1938.
14. Sexton, A.; Whitney, P. G.; Chong, S. F.; Zelikin, A. N.; Johnston, A. P. R.; De Rose, R.; Brooks, A. G.; Caruso, F.; Kent, S. J. A Protective Vaccine Delivery System for *In Vivo* T Cell Stimulation Using Nanoengineered Polymer Hydrogel Capsules. *ACS Nano* **2009**, *3*, 3391–3400.
15. Sexton, A.; Whitney, P. G.; De Rose, R.; Zelikin, A. N.; Chong, S.; Johnston, A. P.; Caruso, F.; Kent, S. J. Nanoengineered Layer-by-Layer Capsules as a Novel Delivery System for HIV Vaccines. *Retrovirology* **2009**, *6*, 2.
16. Chiappetta, D. A.; Hocht, C.; Taira, C.; Sosnik, A. Efavirenz-Loaded Polymeric Micelles for Pediatric Anti-HIV Pharmacotherapy with Significantly Higher Oral Bioavailaibility. *Nanomedicine* **2010**, *5*, 11–23.
17. Tong, W. J.; Gao, C. Y. Multilayer Microcapsules with Tailored Structures for Bio-Related Applications. *J. Mater. Chem.* **2008**, *18*, 3799–3812.
18. Kim, T. W.; Chung, P. W.; Slowing, I. I.; Tsunoda, M.; Yeung, E. S.; Lin, V. S. Y. Structurally Ordered Mesoporous Carbon Nanoparticles as Transmembrane Delivery Vehicle in Human Cancer Cells. *Nano Lett.* **2008**, *8*, 3724–3727.
19. Liu, Z.; Sun, X. M.; Nakayama-Ratchford, N.; Dai, H. J. Supramolecular Chemistry on Water-Soluble Carbon Nanotubes for Drug Loading and Delivery. *ACS Nano* **2007**, *1*, 50–56.
20. Cao, S. W.; Zhu, Y. J.; Ma, M. Y.; Li, L.; Zhang, L. Hierarchically Nanostructured Magnetic Hollow Spheres of Fe_3O_4 and Gamma-Fe_2O_3: Preparation and Potential Application in Drug Delivery. *J. Phys. Chem. C* **2008**, *112*, 1851–1856.
21. Piao, Y.; Kim, J.; Bin Na, H.; Kim, D.; Baek, J. S.; Ko, M. K.; Lee, J. H.; Shokouhimehr, M.; Hyeon, T. Wrap-Bake-Peel process for Nanostructural Transformation from Beta-FeOOH Nanorods to Biocompatible Iron Oxide Nanocapsules. *Nat. Mater.* **2008**, *7*, 242–247.
22. Wei, W.; Ma, G. H.; Hu, G.; Yu, D.; McLeish, T.; Su, Z. G.; Shen, Z. Y. Preparation of Hierarchical Hollow $CaCO_3$ Particles and the Application as Anticancer Drug Carrier. *J. Am. Chem. Soc.* **2008**, *130*, 15808–15810.
23. Zhao, W. R.; Chen, H. R.; Li, Y. S.; Li, L.; Lang, M. D.; Shi, J. L. Uniform Rattle-type Hollow Magnetic Mesoporous Spheres as Drug Delivery Carriers and their Sustained-Release Property. *Adv. Funct. Mater.* **2008**, *18*, 2780–2788.
24. Landfester, K.; Musyanovych, A.; Mailander, V. From Polymeric Particles to Multifunctional Nanocapsules for Biomedical Applications Using the Miniemulsion Process. *J. Polym. Sci., Polym. Chem.* **2010**, *48*, 493–515.
25. Roca, M.; Haes, A. J. Silica-Void-Gold Nanoparticles: Temporally Stable Surf ace-Enhanced Raman Scattering Substrates. *J. Am. Chem. Soc.* **2008**, *130*, 14273–14279.
26. Liang, Z. J.; Susha, A.; Caruso, F. Gold Nanoparticle-Based Core-Shell and Hollow Spheres and Ordered Assemblies Thereof. *Chem. Mater.* **2003**, *15*, 3176–3183.
27. Hah, H. J.; Um, J. I.; Han, S. H.; Koo, S. M. New Synthetic Route for Preparing Rattle-Type Silica Particles with Metal Cores. *Chem. Commun.* **2004**, 1012–1013.
28. Kim, J. Y.; Yoon, S. B.; Yu, J. S. Fabrication of Nanocapsules with Au Particles Trapped inside Carbon and Silica Nanoporous Shells. *Chem. Commun.* **2003**, 790–791.
29. Kim, M.; Sohn, K.; Bin Na, H.; Hyeon, T. Synthesis of Nanorattles Composed of Gold Nanoparticles Encapsulated in Mesoporous Carbon and Polymer Shells. *Nano Lett.* **2002**, *2*, 1383–1387.
30. Kamata, K.; Lu, Y.; Xia, Y. N. Synthesis and Characterization of Monodispersed Core-Shell Spherical Colloids with Movable Cores. *J. Am. Chem. Soc.* **2003**, *125*, 2384–2385.
31. Lee, J.; Park, J. C.; Bang, J. U.; Song, H. Precise Tuning of Porosity and Surface Functionality in Au@SiO_2 Nanoreactors for High Catalytic Efficiency. *Chem. Mater.* **2008**, *20*, 5839–5844.
32. Lee, J.; Park, J. C.; Song, H. A Nanoreactor Framework of a Au@SiO_2 Yolk/Shell Structure for Catalytic Reduction of p-nitrophenol. *Adv. Mater.* **2008**, *20*, 1523–1528.
33. Skirtach, A. G.; Antipov, A. A.; Shchukin, D. G.; Sukhorukov, G. B. Remote Activation of Capsules Containing Ag Nanoparticles and IR Dye by Laser Light. *Langmuir* **2004**, *20*, 6988–6992.
34. Kim, J.; Lee, J. E.; Lee, J.; Yu, J. H.; Kim, B. C.; An, K.; Hwang, Y.; Shin, C. H.; Park, J. G.; Hyeon, T. Magnetic Fluorescent Delivery Vehicle using Uniform Mesoporous Silica Spheres Embedded with Monodisperse Magnetic and Semiconductor Nanocrystals. *J. Am. Chem. Soc.* **2006**, *128*, 688–689.
35. Gaponik, N.; Radtchenko, I. L.; Gerstenberger, M. R.; Fedutik, Y. A.; Sukhorukov, G. B.; Rogach, A. L. Labeling of Biocompatible Polymer Microcapsules with Near-Infrared Emitting Nanocrystals. *Nano Lett.* **2003**, *3*, 369–372.
36. Zhu, Y. F.; Kockrick, E.; Ikoma, T.; Hanagata, N.; Kaskel, S. An Efficient Route to Rattle-Type Fe_3O_4@SiO_2 Hollow Mesoporous Spheres Using Colloidal Carbon Spheres Templates. *Chem. Mater.* **2009**, *21*, 2547–2553.
37. Zhu, Y. F.; Ikoma, T.; Hanagata, N.; Kaskel, S. Rattle-Type Fe_3O_4@SiO_2 Hollow Mesoporous Spheres as Carriers for Drug Delivery. *Small* , *6*, 471–478.
38. Zhang, L.; Qiao, S. Z.; Jin, Y. G.; Chen, Z. G.; Gu, H. C.; Lu, G. Q. Magnetic Hollow Spheres of Periodic Mesoporous Organosilica and Fe_3O_4 Nanocrystals: Fabrication and Structure Control. *Adv. Mater.* **2008**, *20*, 805–809.
39. Angelatos, A. S.; Radt, B.; Caruso, F. Light-Responsive Polyelectrolyte/Gold Nanoparticle Microcapsules. *J. Phys. Chem. B* **2005**, *109*, 3071–3076.
40. Huang, X. L.; Teng, X.; Chen, D.; Tang, F. Q.; He, J. Q. The Effect of The Shape of Mesoporous Silica Nanoparticles on Cellular Uptake and Cell Function. *Biomaterials* **2010**, *31*, 438–448.

41. Mitragotri, S.; Lahann, J. Physical Approaches to Biomaterial Design. *Nat. Mater.* **2009**, *8*, 15–23.
42. Zhao, W. R.; Gu, J. L.; Zhang, L. X.; Chen, H. R.; Shi, J. L. Fabrication of Uniform Magnetic Nanocomposite Spheres with a Magnetic Core/Mesoporous Silica Shell Structure. *J. Am. Chem. Soc.* **2005**, *127*, 8916–8917.
43. Shi, D. L.; Cho, H. S.; Chen, Y.; Xu, H.; Gu, H. C.; Lian, J.; Wang, W.; Liu, G. K.; Huth, C.; Wang, L. M.; et al. Fluorescent Polystyrene-Fe_3O_4 Composite Nanospheres forIn Vivo Imaging and Hyperthermia. *Adv. Mater.* **2009**, *21*, 2170–2173.
44. Lu, C. W.; Hung, Y.; Hsiao, J. K.; Yao, M.; Chung, T. H.; Lin, Y. S.; Wu, S. H.; Hsu, S. C.; Liu, H. M.; Mou, C. Y.; et al. Bifunctional Magnetic Silica Nanoparticles for Highly Efficient Human Stem Cell Labeling. *Nano Lett.* **2007**, *7*, 149–154.
45. Lee, J. E.; Lee, N.; Kim, H.; Kim, J.; Choi, S. H.; Kim, J. H.; Kim, T.; Song, I. C.; Park, S. P.; Moon, W. K.; et al. Uniform Mesoporous Dye-Doped Silica Nanoparticles Decorated with Multiple Magnetite Nanocrystals for Simultaneous Enhanced Magnetic Resonance Imaging, Fluorescence Imaging, and Drug Delivery. *J. Am. Chem. Soc.* **2010**, *132*, 552–557.
46. Stober, W.; Fink, A.; Bohn, E. Controlled Growth of Monodisperse Silica Spheres in Micron Size Range. *J. Colloid Interface Sci.* **1968**, *26*, 62–69.
47. Morishige, K.; Tateishi, N. Adsorption Hysteresis in Ink-Bottle Pore. *J. Chem. Phys.* **2003**, *119*, 2301–2306.
48. Park, S. J.; Kim, Y. J. Size-Dependent Shape Evolution of Silica Nanoparticles into Hollow Structures. *Langmuir* **2008**, *24*, 12134–12137.
49. Grzelczak, M.; Correa-Duarte, M. A.; Liz-Marzan, L. M. Carbon Nanotubes Encapsulated in Wormlike Hollow Silica Shells. *Small* **2006**, *2*, 1174–1177.
50. Chen, D.; Li, L. L.; Tang, F. Q.; Qi, S. O. Facile and Scalable Synthesis of Tailored Silica "Nanorattle" Structures. *Adv. Mater.* **2009**, *21*, 3804–3807.
51. Tao, Z. M.; Toms, B.; Goodisman, J.; Asefa, T. Mesoporous Silica Microparticles Enhance the Cytotoxicity of Anticancer Platinum Drugs. *ACS Nano* **2010**, *4*, 789–794.
52. Conner, S. D.; Schmid, S. L. Regulated Portals of Entry into The Cell. *Nature* **2003**, *422*, 37–44.
53. Marsh, M.; McMahon, H. T. Cell Biology-The Structural Era of Endocytosis. *Science* **1999**, *285*, 215–220.
54. Guo, L. M.; Zhang, L. X.; Zhang, J. M.; Zhou, J.; He, Q. J.; Zeng, S. Z.; Cui, X. Z.; Shi, J. L. Hollow Mesoporous Carbon Spheres-an Excellent Bilirubin Adsorbent. *Chem. Commun.* **2009**, 6071–6073.
55. Slowing, I. I.; Wu, C. W.; Vivero-Escoto, J. L.; Lin, V. S. Y. Mesoporous Silica Nanoparticles for Reducing Hemolytic Activity Towards Mammalian Red Blood Cells. *Small* **2009**, *5*, 57–62.
56. Sun, C.; Fang, C.; Stephen, Z.; Veiseh, O.; Hansen, S.; Lee, D.; Ellenbogen, R. G.; Olson, J.; Zhang, M. Q. Tumor-Targeted Drug Delivery and MRI Contrast Enhancement by Chlorotoxin-Conjugated Iron Oxide Nanoparticles. *Nanomedicine* **2008**, *3*, 495–505.
57. Na, H. B.; Song, I. C.; Hyeon, T. Inorganic Nanoparticles for MRI Contrast Agents. *Adv. Mater.* **2009**, *21*, 2133–2148.
58. Lebold, T.; Jung, C.; Michaelis, J.; Brauchle, C. Nanostructured Silica Materials As Drug-Delivery Systems for Doxorubicin: Single Molecule and Cellular Studies. *Nano Lett.* **2009**, *9*, 2877–2883.
59. Zhu, Y. F.; Shi, J. L.; Li, Y. S.; Chen, H. R.; Shen, W. H.; Dong, X. P. Storage and Release of Ibuprofen Drug Molecules in Hollow Mesoporous Silica Spheres with Modified Pore Surface. *Microporous Mesoporous Mater.* **2005**, *85*, 75–81.
60. Vallet-Regi, M; Balas, F.; Arcos, D. Mesoporous Materials for Drug Delivery. *Angew. Chem. Int. Ed.* **2007**, *46*, 7548–7558.
61. Vallet-Regi, M.; Ramila, A.; del Real, R. P. Perez-Pariente, A New Property of MCM-41: Drug Delivery System. *Chem. Mater.* **2001**, *13*, 308–311.
62. Slowing, I. I.; Vivero-Escoto, J. L.; Wu, C. W.; Lin, V. S. Y. Mesoporous Silica Nanoparticles as Controlled Release Drug Delivery and Gene Transfection Carriers. *Adv. Drug Delivery Rev.* **2008**, *60*, 1278–1288.
63. Yoshida, M.; Shiojima, I.; Ikeda, H.; Komuro, I. Chronic Doxorubicin Cardiotoxicity is Mediated by Oxidative DNA Damage-ATM-p53-Apoptosis Pathway and Attenuated by Pitavastatin Through The Inhibition of Rac1 Activity. *J. Mol. Cell. Cardiol.* **2009**, *47*, 698–705.
64. dos Santos, R. A.; Jordao, A. A.; Vannucchi, H.; Takahashi, C. S. Protection of Doxorubicin-Induced DNA Damage by Sodium Selenite and Selenomethionine in Wistar Rats. *Nutr. Res. (N.Y.)* **2007**, *27*, 343–348.
65. Kim, J.; Lee, J. E.; Lee, S. H.; Yu, J. H.; Lee, J. H.; Park, T. G.; Hyeon, T. Designed Fabrication of a Multifunctional Polymer Nanomedical Platform for Simultaneous Cancer-Targeted Imaging and Magnetically Guided Drug Delivery. *Adv. Mater.* **2008**, *20*, 478–483.
66. Jain, P. K.; El-Sayed, I. H.; El-Sayed, M. A. Au Nanoparticles Target Cancer. *Nano Today* **2007**, *2*, 18–29.
67. Hu, Y.; Chen, Q.; Ding, Y.; Li, R. T.; Jiang, X. Q.; Liu, B. R. Entering and Lighting Up Nuclei Using Hollow Chitosan-Gold Hybrid Nanospheres. *Adv. Mater.* **2009**, *21*, 3639–3643.